

See discussions, stats, and author profiles for this publication at: <https://www.researchgate.net/publication/243374236>

Electrochemistry of Molecule-like Au₂₅ Nanoclusters Protected by Hexanethiolate

ARTICLE *in* THE JOURNAL OF PHYSICAL CHEMISTRY C · MAY 2009

Impact Factor: 4.77 · DOI: 10.1021/jp901118t

CITATIONS

23

READS

67

4 AUTHORS, INCLUDING:



Rafael Madueño

University of Cordoba (Spain)

24 PUBLICATIONS 541 CITATIONS

[SEE PROFILE](#)



Manuel Blázquez

University of Cordoba (Spain)

76 PUBLICATIONS 883 CITATIONS

[SEE PROFILE](#)



Teresa Pineda

University of Cordoba (Spain)

41 PUBLICATIONS 325 CITATIONS

[SEE PROFILE](#)

Electrochemistry of Molecule-like Au₂₅ Nanoclusters Protected by Hexanethiolate

Daniel García-Raya, Rafael Madueño, Manuel Blázquez, and Teresa Pineda*

Departamento de Química Física y Termodinámica Aplicada, Universidad de Córdoba, Campus de Rabanales, Ed. Marie Curie, E-14071 Córdoba, Spain

Received: February 6, 2009; Revised Manuscript Received: March 19, 2009

Near-monodisperse fractions of hexanethiol-protected gold nanoclusters (Au(25) and Au(144)) have been obtained by using a variation of the two-phase Brust method based on constant low temperature (4 °C) and control of the stirring conditions during the synthesis procedure. The size and dispersity of the Au₂₅(SC₆)₁₈ and Au₁₄₄(SC₆)₅₉ nanoclusters are determined by electrochemical means. The two first oxidation steps for the molecule-like Au₂₅(SC₆)₁₈ clusters are quasi-reversible, and the electron transfer rate constants and diffusion coefficients have been determined by cyclic voltammetry and electrochemical impedance spectroscopy. The electrochemical behavior of these nanoclusters in different solvents can be explained by using the model described by Girault et al. (*J. Phys. Chem. B* 2006, 110, 21460; 2005, 109, 23925.) that considers the contribution of the bulk solvent relative permittivity on the charging energy values. Electrolyte ions and solvent molecule penetration must be taken into account to explain the deviation of the charging energy value in solvents such as toluene, whose relative permittivity is close to that of the protecting monolayer. The HOMO–LUMO energy gap measured by electrochemical and optical spectroscopy means does not show any influence of the solvent nature as observed for Au₂₅(PhC₂S)₁₈.

Introduction

The development of nanoparticle stabilizing chemistry has enabled direct electrochemical observations on solutions of nanoparticles. According to the potential-driven electron transfer that the metal nanoparticles may undergo in voltammetry at a working electrode and its size-dependent changes, three regimes can be distinguished: bulk-continuum, quantized double layer (QDL) charging, and molecule-like.¹ In this sense, electrochemical experiments offer a straightforward way to measure MPC size and dispersity as each cluster has its own charging signature that is dependent on core size, nature of protecting monolayer, and the dispersing medium.^{1–7}

The molecule-like phenylethanethiolate-protected Au₂₅ cluster (Au₂₅(PhC₂S)₁₈) was isolated on the basis of a strong solubility differentiation from larger nanoparticles.⁸ Recent X-ray structure determination of these nanoparticles showed an unusual geometry consisting of a 13-atom gold icosahedron core with a further 12 Au atoms stellating on its faces. The 12 outer Au atoms are bonded to the thiolate ligands in a staple motif and may be influenced by aurophilic bonding. The thiolate ligand attachment sites are symmetrically distributed on the surface to ensure complete passivation of the nanoparticle.⁹ Thus, the staple motifs may play a role during nanoparticle synthesis and exemplify the “divide and protect” model¹⁰ in which oligomeric aurous Au(I)–thiolate complexes interact weakly with the surface atoms of the core.¹¹

The electrochemical formal potentials for the first one-electron reduction and one-electron oxidation of Au₂₅(PhC₂S)₁₈ are separated by 1.65 (±0.03) V. The large electrochemical potential spacing, the electrochemical energy gap, is consistent with a molecule-like, discretized electronic energy level structure for these Au₂₅(PhC₂S)₁₈. The observed electrochemical potentials are affected by the relative degrees of solvent dipole and

electrolyte ion-pairing stabilization of the electron donor and acceptor states, an effect known as “charging energy”. The charging energy normally enhances the electrochemical energy gap relative to the optical band gap energy. Thus, the correction of the electrochemical energy gap for charging energy gives the HOMO–LUMO gap energy somewhat above 1.3 eV, which corresponds to the observed 1.33 eV optical absorption onset of these nanoclusters.¹² It was found that, while the charging energy decreases strongly as the solvent mix becomes more polar, the electrochemical energy gap and the HOMO–LUMO gap energy change only moderately. In fact, the first oxidation and first reduction formal potentials shift positively in a more polar solvent environment, although greater changes are observed in the latter process.^{2,12} This higher sensitivity of the reduction potential to the change in solvent may include other effects different from solvent polarity as can be the stabilization by the hydrophobic electrolyte cation. This behavior is explained as being due to a combination of the ligand shell dielectric constant and that of the solvent that should also penetrate the ligand shell in some degree, a phenomenon that is referred to as solvation/penetration.^{12,13}

On the other hand, the inclusion of substituents on the Au₂₅(PhC₂SX)₁₈ shell has effects on the redox formal potentials in a way that favors reduction and disfavors oxidation. However, the substituents effect does not produce changes in the HOMO–LUMO gap energy.¹⁴ Whereas the electron-withdrawing or electron-donating substituents cause shifts in the voltammetric formal potential as much as 0.45 V,¹⁴ the exchange of PhC₂S ligands by peptides that can form stiff helices that generate a substantial dipole moment along the helical axis produces substantial positive shifts in the first and second oxidation peaks of this MPC.¹⁵ The extent of the potential shifts (0.7–0.8 V) depends on the number of thiolated peptide ligands exchanged into the MPC monolayer.

Recently, Girault et al.^{16,17} considered both theoretically and experimentally the effect of organic solvents on the redox

* To whom correspondence should be addressed. Telephone: +34-957-218646. Fax: +34-957-218618. E-mail: tpineda@uco.es.

properties of MPCs ($\text{Au}_{140}(\text{S}(\text{CH}_2)_5\text{CH}_3)_{53}$), showing clearly that the potential separation between neighboring redox states increases with decreasing the relative permittivity of the solvent, thus providing concrete evidence that the organic solvent has a significant effect on the redox properties of MPCs, despite the fact that the monolayer acts as a protecting layer of the metal core. Moreover, they considered that the solvent penetration in the protecting layer and electrolyte ion binding can change the effective dielectric constant and thickness of the monolayer and can also shift the redox potential of MPCs if the binding process is taken as a chemical reaction coupled to the MPC redox reaction.¹⁶ The ion permeability of monolayers in MPCs affects the capacitance and the charging energy, although the ion penetration is tuned by the charge and size of the ions and the permittivity of the solvent.¹⁸

In this work, we synthesized gold nanoclusters by following a variation of the two-phase Brust method.¹⁹ By controlling the synthesis temperature at 4 °C during the entire process, we obtained near-monodisperse preparations of Au(25) and Au(144) nanoclusters using hexanethiol as protecting ligand. The focus of this study is on the effect of the solvent relative permittivity on the electrochemical properties of the smaller cluster isolated, the Au(25) hexanethiolate-protected gold nanoclusters, by using dichloroethane (DCE), dichloromethane (DCM), chlorobenzene (CB), and toluene (TOL) solvents. By studying the cyclic voltammetry, differential pulse voltammetry, and electrochemical impedance spectroscopy of these MPCs, the electron transfer rate constants of the two first oxidation processes as well as the diffusion coefficients of these species were determined.

Experimental Section

Chemicals. Hexanethiol (99%), tetra-*n*-octylammonium bromide (TOABr) (98%), sodium borohydride (99%), lithium bis(thifluoromethanesulfon)imide (LiTf_2N), and tetrahexylammonium chloride (THACl) were used as received from Aldrich-Sigma. DCE, DCM, CB, TOL, acetonitrile, and ethanol (Chromasolv for HPLC) were also from Aldrich-Sigma and were dried with molecular sieves before using. Hydrogen tetrachloroaurate trihydrate (from 99.999% pure gold) was prepared using a literature procedure²⁰ and stored in a freezer at -20 °C. Deionized water (18 MΩ) from milli-Q system was used in all the experiments.

Synthesis of Tetrahexylammonium Bis(trifluoromethylsulfonyl)-imide (THATf₂N).¹⁶ THATf₂N ionic liquid was prepared by metathesis of THACl and LiTf₂N in a molar ratio of 1:1 in water under vigorous stirring. The reaction was allowed to proceed overnight and resulted in a milky mixture, to which DCM was added. The mixing liquids were stirred overnight. Then, the DCM layer was separated with a separating funnel, and the water layer was washed with DCM as described above, three times. The DCM solution containing THATf₂N was rotary-evaporated to remove DCM. The viscous liquid remaining in the round-bottom flask included THATf₂N and possibly unreacted residues. The obtained ionic liquids were washed with a large amount of ultrapure water and then dried in a vacuum at 100 °C.

Synthesis of Au-MPCs. Hexanethiolate-protected gold nanoclusters were prepared using a modified Brust two-phase procedure,¹⁹ as follows. Tetrachloroaurate (2 g) was phase-transferred from aqueous solution to toluene using TOABr (3.60 g). The yellow aqueous solution was quickly cleared, and the toluene solution became dark red as tetrachloroaurate was transferred into it. A 5-fold molar excess of hexanethiol (3.6 mL) relative to gold was then added to the separated toluene

phase. The solution was stirred (60 rpm) until it became colorless, and, in this moment, a freshly prepared aqueous solution of sodium borohydride (1.94 g) (10-fold molar excess with respect to Au reactant) was added under stirring. The reduction reaction was maintained for 30 min, and, after that, the phases were separated and the toluene phase was repeatedly washed with milli-Q water and rotary-evaporated to produce a black slurry. Ethanol was then added to this product and was left overnight under stirring. The suspension was filtered, and the ethanol insoluble fraction (MPC 1) was washed with copious amounts of ethanol. The ethanol soluble fraction was rotary-evaporated, and acetonitrile was added to the black slurry that, after 1–2 h of stirring, was allowed to stand overnight. The supernatant was removed, and the precipitate was washed with acetonitrile and dried (MPC 2). The synthesis procedure was carried out in a cold room at 4 °C, and all the solutions were equilibrated at this temperature before use.

Electrochemistry. Cyclic voltammetry (CV), differential pulse voltammetry (DPV), and electrochemical impedance spectroscopy (EIS) were done with an Autolab (Eco Chemie model Pgstat 20) instrument attached to a PC with proper software (GPES and FRA) for total control of the experiment and data acquisition. The CV and EIS data were fitted through the use of the Eco Chemie digital simulation and frequency response analyzer (FRA) 4.9 software. To determine the heterogeneous parameters (in addition to the Nicholson method²¹), the experimental CV curves were digitally simulated with the DigiSim 3.03 package. A three-electrode arrangement was used, in which a silver wire was used as a quasi-reference electrode (AgQRE) and a platinum wire as counter electrode. The working electrodes were either glassy carbon or platinum disk-shape macro- (1.6-mm diameter) or microelectrodes (25-μm diameter) from Bioanalytical Systems. The working electrodes were polished with 0.05-μm Al₂O₃ slurry and then rinsed and sonicated in Milli-Q water and dried before measurements. The platinum electrodes were cycled in 0.5 M H₂SO₄ until the appropriate i-E profile was obtained. The MPCs (0.08 mM) were dissolved in the various organic media containing 0.1 M THATf₂N, and nitrogen was bubbled for 10 min before measurements.

UV–Visible Spectroscopy. UV–visible spectra were collected with a JASCO UV–visible–NIR (model V-570) spectrometer.

High-Resolution Transmission Electronic Microscopy (HR-TEM). HR-TEM images were obtained with a JEOL JEM 2010 instrument operating at 80–200 kV and analyzed using Image Pro Plus software. Samples were prepared by casting and evaporating a droplet of MPC solution (2–3 mg/mL) onto Formvar-coated Cu grids (400 mesh, Electron Microscopy Sciences).

Results and Discussion

The monodispersity of the as-prepared MPC 1 and MPC 2 fractions was first assayed by electrochemical means since the resolution of single-electron charging peaks is indicative of this MPC's property.^{7,22–24}

Figure 1 shows the DPV and CV of the synthesized MPC1 and MPC2 in DCM. The DPV of MPC1 (Figure 1a) exhibits the typical molecule-like behavior.¹ The first oxidation and first reduction peaks of the nanoparticle lie at 0.02 and -1.62 V vs the AgQRE electrode, and the 1.64 V separation between these peaks corresponds to the electrochemical energy gap for this MPC. These values are similar to those found for $\text{Au}_{38}(\text{SC}_6)_{24}$ nanoclusters.^{3,24} However, taking into account the recent cor-

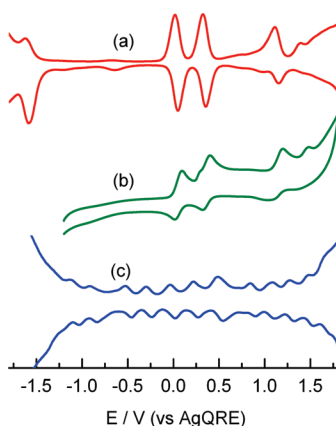


Figure 1. Electrochemical responses for MPC solutions measured with a GC electrode in DCM in 0.1 M THATf₂N. (a) DPV and (b) CV of MPC1 and (c) DPV of MPC2.

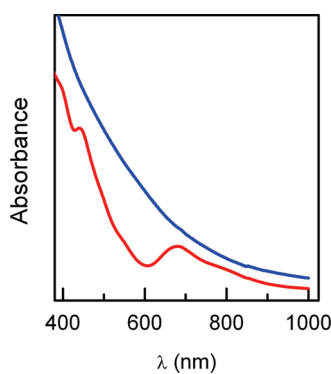


Figure 2. UV-visible spectrum of (red) MPC1 and (blue) MPC2 fractions in DCE solution. The spectra have been offset for clarity.

rection of the size of the nanoclusters showing these electrochemical properties,^{1,25} we assume that the MPC1 fraction corresponds to Au₂₅(SC₆)₁₈.

The first electron transfer from the HOMO is followed by a second step at 0.31 V that is more positive and corresponds to the Au₂₅^{0/-1} (Ox1) and Au₂₅^{+1/0} (Ox2) couples, respectively. From these peaks, an electrochemical estimate of the Au₂₅(SC₆)₁₈ HOMO–LUMO gap energy of 1.33 V can be made. This value is similar to that obtained for Au₂₅–MPC protected by phenylethanethiol (Au₂₅(SCH₂CH₂Ph)₁₈),¹ even though the oxidation and reduction potentials are lower. Moreover, it coincides with the optical HOMO–LUMO gap energy as measured at the optical absorbance edge for this MPC^{1,3,8,12,14,15,24,26} (Figure 2). Moreover, the shape of this spectrum with a band at 680 nm (1.80 eV) and shoulders at 450 nm (2.75 eV) and 395 nm (3.1 eV) agrees with that theoretically proposed for Au(25) clusters that suffer strong quantum size effects and show multiple molecular-like transitions. This optical behavior is different from that of gold nanocrystals (>3 nm) that show surface plasmon resonance transitions at 520 nm (~2.4 eV). The peak at 680 nm has been assigned to a transition entirely due to the electronic and geometric structure of the Au₁₃ core that plays an important role in the optical properties of this cluster.²⁷

On the other hand, the DPV of MPC2 (Figure 1c) shows the typical shape of QDL charging voltammetry. In fact, 11 evenly spaced peaks (average separation 0.26 V) corresponding to the charge injection to the metal core are observed. This QDL voltammetry is similar to that reported for Au₁₄₀(SC₆)₅₃^{1,5} (recently reported as Au₁₄₄(SC₆)₅₉²⁸), as well as the optical spectrum (Figure 2).

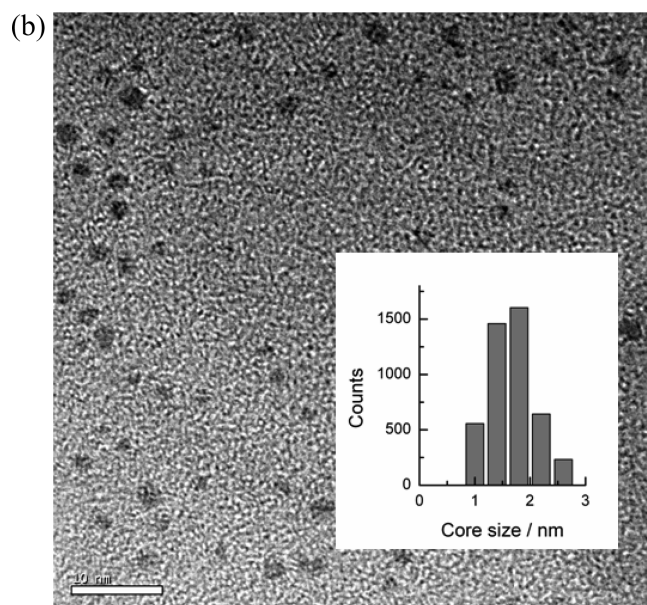
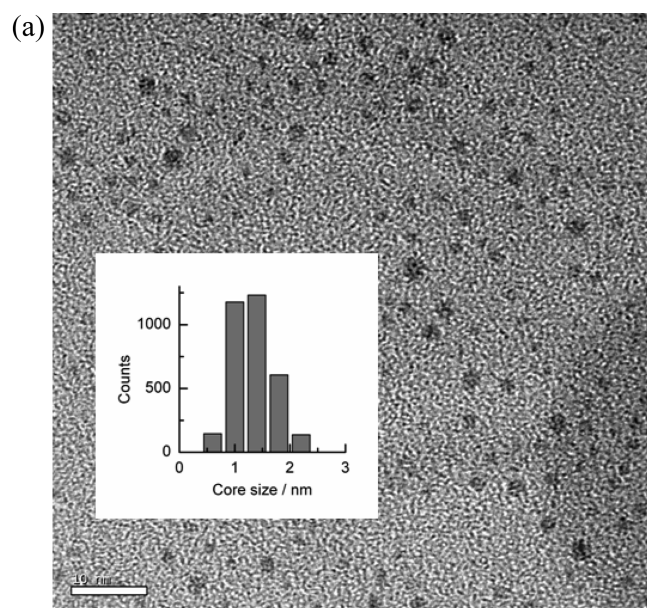


Figure 3. TEM images and corresponding histograms of the (a) MPC1 and (b) MPC2 fractions. Scale bars are 10 nm.

An additional characterization of these MPCs comes from TEM images (Figure 3). As can be observed, the average sizes of these nanoclusters are 1.2 ± 0.5 and 1.6 ± 0.5 nm for MPC 1 and MPC 2, respectively. Thus, the synthesis procedure followed in this work yields two main fractions of nanoclusters of Au₂₅ and Au₁₄₄ that each presents a narrow distribution of sizes. It is possible that the control of the temperature of synthesis has helped in narrowing the sizes. Moreover, the preparation of Au₂₅ nanoclusters protected by hexanethiolate^{3,8,24,29} has been shown to be more difficult than those protected by phenylethanethiol^{3,12,30,31} and other ligands as glutathione.^{32,33} In fact, the synthesis methods based on hexanethiolate yield in most cases Au₃₈ nanoclusters, as reported by Quinn et al.,^{5,7} who found a HOMO–LUMO gap energy of 0.9 V. Therefore, as reported by Murray,¹ the electrochemical method can be properly used as a means to identify nanocluster core sizes and to prove MPC size and monodispersity.

The Ox1 and Ox2 redox reactions are well-behaved in terms of chemical reversibility as demonstrated by isolating these

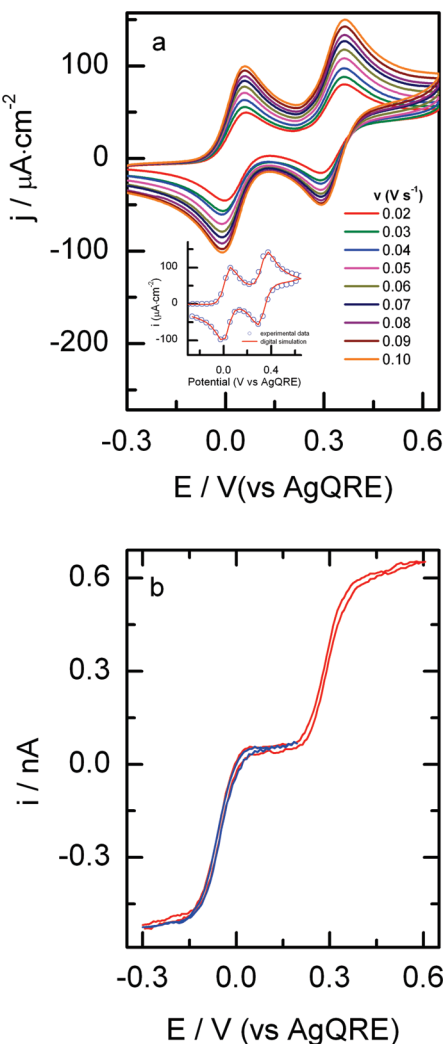


Figure 4. Electrochemical responses of 0.08 mM Au₂₅(SC₆)₁₈ in DCM solution containing 0.1 M of THATf₂N. (a) Background-subtracted CV recorded at different scan rates with a GC electrode (3-mm diameter). Inset: Experimental (blue circles) and simulated (red solid line) cyclic voltammetry curve at 0.1 V/s. (b) Microelectrode voltammetry recorded at 0.1 V/s with a Pt electrode (25-μm diameter).

electron transfer redox processes (Figure 4). The cyclic voltammograms (either with glassy carbon or with Pt macroelectrodes) show two quasi-reversible peaks that, at low scan rates, exhibit a separation between the anodic and cathodic peak potentials of ~60 mV, although ΔE_p increases with increasing scan rates. The electron transfer rate constants for peaks Ox1 and Ox2 were determined from the scan rate dependence of the oxidation currents as well as by digital simulation of the cyclic voltammograms and result of 0.017 and 0.021 cm/s, respectively.

The microelectrode voltammetry for the isolated Ox1 and Ox2 processes shows the quasi-reversible characteristics of these electron transfer processes. The current plateau for the Ox1 couple lies nearly at zero current as reported for Au₂₅(PhC₂S)₁₈.³⁴ This is the potential of the nanoparticle PZC, and at this potential the interfacial solution contains primarily the Au⁰ species.¹ As the waves are well separated along the potential axis, they can be analyzed individually. For a disk microelectrode, the diffusion-controlled limiting current is proportional to the radius of the microelectrode (a), the diffusion coefficient (D), and the concentration of the redox species:

$$I_s = 4\pi F D a c \quad (1)$$

Therefore, from the microelectrode voltammograms, one can derive the diffusion coefficients of the Ox1 and Ox2 species of Au₂₅(SC₆)₁₈ MPCs. The values obtained are 3.07×10^{-6} and 3.12×10^{-6} cm²/s, respectively, in agreement with the value of 3.9×10^{-6} cm²/s determined by using the Stokes–Einstein equation ($D = k_B T / 6\pi r \eta$, where k_B is the Boltzmann constant, and η is the viscosity of the solvent, and r is the molecular radius).

Figure 5 shows the impedance spectra plotted as Nyquist plots for the Ox1 and Ox2 redox couples. The spectra show a low frequency straight line with a very small semicircle at high frequencies, indicating a diffusion-controlled process for the redox couple. These results parallel those of cyclic voltammetry where a quasi-reversible behavior is obtained. The impedance spectra are fitted to a standard Randles's equivalent circuit consisting of a parallel combination of a capacitor represented by C and a faradaic impedance Z_f in series with the uncompensated solution resistance, R_s . The faradaic impedance, Z_f , is a series combination of charge transfer resistance, R_{ct} , and the Warburg impedance, W . The electron transfer rate constant, k_{app} , can be estimated from these data by using eq 2:

$$R_{CT} = \frac{RT}{n^2 \cdot F^2 \cdot A \cdot k_{app} \cdot c} \quad (2)$$

where R is the gas constant, T is the temperature, F is Faraday's constant, n is the number of electrons, A is the area of the electrode, and c is the concentration of the redox couple. Values of 0.022 and 0.015 cm/s for the spectra recorded at 0.03 and 0.32 V, respectively, were obtained that are in agreement with those determined by digital simulation of the corresponding voltammetric curves.

These values are of the same order as those determined for Au₂₅(PhC₂S)₁₈² in the same solvent. However, it was reported that the electron transfer reactions involving MPCs are faster than those between conventional redox species³⁴ and the electron transfer rate is dependent mostly on the composition of the protecting layer and not on differences in the core metal.³⁵ In fact, the equilibrium or rest potential of the MPC solution can be described in terms of the Nernst equation.^{36,37} In this sense,

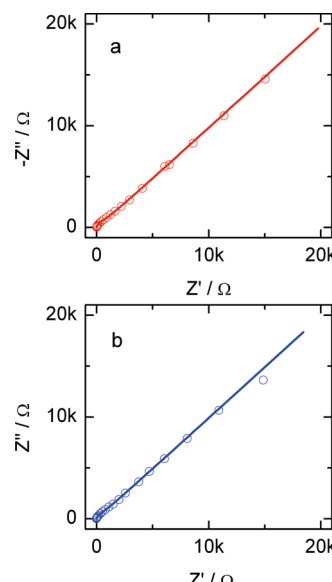


Figure 5. Nyquist plots of the Au₂₅(SC₆)₁₈ in DCM with 0.1 M THATf₂N recorded at (a) 0.03 V (Ox1) and (b) 0.32 V (Ox2). (○) Experimental data; (—) fit to the Randles equivalent circuit.

Quinn et al.³⁸ used the scanning electrochemical microscopy technique to obtain reliable kinetics data for the Au(140) MPCs, and they found values of the rate constant >0.1 cm/s at the metal–electrolyte interface, whereas they were lower at the liquid–liquid interface.

Solvent Effect on Redox Properties of $\text{Au}_{25}(\text{SC}_6)_{18}$. The charging energy (energy required to gain/lose an extra electron) of the MPCs is known to be affected by the relative degrees of solvent dipole and electrolyte ion-pairing stabilization of the donor and acceptor states. The model proposed by Girault et al.¹⁶ that considers the MPC as a charged metallic core surrounded by two dielectric layers, the intrinsic protecting layer and the medium outside constituted by the solvent, predicts an effect of the solvent dielectric constant, ϵ_s , on the voltage separation, ΔV , between successive single electron transfer events given by eq 3.

$$\Delta V = \frac{e}{4\pi\epsilon_0(r_o + d)} \left(\frac{d}{\epsilon_d r_o} + \frac{1}{\epsilon_s} \right) \quad (3)$$

where r_o and d are the radius of the metallic core and the monolayer thickness, respectively, and ϵ_d is the relative permittivity of the protecting monolayer.

These effects were demonstrated by studying the voltammetry, DPV as well as microelectrode cyclic voltammetry, of $\text{Au}_{140}(\text{SC}_6)_{53}$ in solvents in a range of different relative permittivities performing a compromise between nanocluster and supporting electrolyte solubility. They chose solvents in the low relative permittivity range such as DCE, DCM, CB, and TOL (relative permittivities are 10.37, 8.93, 5.69, and 2.38, respectively), which is where these MPCs are soluble. The use of an ionic liquid (THATf₂N) as supporting electrolyte enabled the electrochemical measurements in TOL at room temperature for the first time.¹⁶ In this study, they found that ΔV , that is, the charging energy, increases as the relative permittivity of the solvent decreases, in agreement with eq 3. An important change in this magnitude was also found for $\text{Au}_{25}(\text{PhC}_2\text{S})_{18}$,² when studied in the solvents DCM and DMF. The oxidation formal potentials displace to positive values and the charging energy decreases when passing from DCM to DMF, also in agreement with eq 3.

In a similar way, we present the study of the effects of the solvent relative permittivity on the electrochemical properties of the $\text{Au}_{25}(\text{SC}_6)_{18}$ synthesized in this work. Figure 6a shows the DPVs of the $\text{Au}_{25}(\text{SC}_6)_{18}$ in DCE, DCM, CB, and TOL. The use of solvents of higher relative permittivity was precluded because, contrary to the $\text{Au}_{25}(\text{PhC}_2\text{S})_{18}$, the MPCs protected by hexanethiol were not soluble in those solvents in a concentration that the electrochemical signals obtained were appropriate. The DPVs recorded in the four solvents employed show the same number of peaks but, as can be observed, a change in the potentials to more positive (oxidation) or negative values (reduction) as the relative permittivity decreases was produced. The important parameters in the molecule-like voltammetry¹ are the charging energy (Ox1–Ox2 peak potentials), the electrochemical energy gap (Red1–Ox1 peak potentials), and the HOMO–LUMO gap energy. These values are also plotted in Figure 6.

While the charging energy and the electrochemical energy gap increase with decreasing solvent permittivity, the HOMO–LUMO energy gap decreases. The changes observed on the charging energy follow a trend similar to that found for hexanethiolate-protected Au(140) MPCs.¹⁶ In fact, the experimental data corresponding to the solvents of higher relative permittivity are close to the theoretical line obtained from eq 3

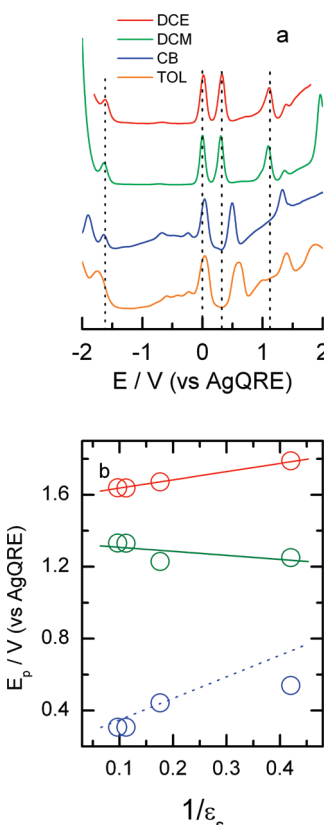


Figure 6. (a) DPV of the $\text{Au}_{25}(\text{SC}_6)_{18}$ in different solvent solution containing 0.1 M THATf₂N. (b) Changes of the charging energy (blue ○), electrochemical energy gap (red ○), and HOMO–LUMO gap energy (green ○) with the inverse of the solvent relative permittivity. The blue dotted trace corresponds to the theoretical curve of eq 3. The solid lines are linear fits to the experimental data.

with $r_o = 0.65$ nm, $d = 0.55$ nm,^{9,39} and $\epsilon_d = 4.436$.⁴⁰ Moreover, the charging energy obtained in TOL is lower than the predicted value as it was obtained in the case of Au(140). In this case, an anomalous behavior was also found in TOL that was ascribed to the effects of possible solvent penetration in the protecting monolayer and electrolyte ion binding. Within the solvents used in this work, TOL has the value of the solubility parameter close to that of the hydrocarbon chain;⁴¹ thus, it can penetrate the protecting hexanethiol layer in more extension than the rest of the solvents used.⁴² The solvent penetration can decrease the value of ϵ_d and increase the monolayer thickness as proposed for dodecanethiolate-protected gold nanoparticles⁴³ and, thus, provoke a decrease of the charging energy (eq 3). Thus, although the solvent molecules can penetrate the ligand shell in some extension due to its sharp curvature¹² this effect is somewhat higher in the case of TOL. Moreover, the effects of ion penetration need to be taken into account, and the conclusions of the study of Quinn et al.¹⁸ indicating that solvents of a dielectric constant close to that of the monolayer facilitate ion penetration into the monolayer can be applied to the present case for TOL.

Nevertheless, the HOMO–LUMO gap energy shows a slight decrease with the solvent relative permittivity (from 1.33 to 1.25 eV), although the magnitude is very small to be taken into account as the estimate of charging energy is rough, as previously discussed.¹²

The UV–visible spectra of the $\text{Au}_{25}(\text{SC}_6)_{18}$ MPCs in the four solvents are shown in Figure 7. The optical properties of Au(25) clusters were recently studied from a theoretical point of view,^{27,44,45} and the results clearly demonstrate that the cluster

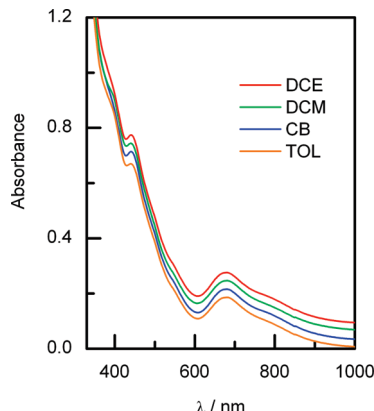


Figure 7. UV-visible absorption spectra of Au₂₅(SC₆)₁₈ MPCs in different solvents. The spectra have been offset for clarity.

structure plays an important role. The absorption spectrum appears to be a property of the core and not of the surface.^{27,45} Thus, the similar Au₂₅(SC₆)₁₈ MPC spectra in the different solvents as observed for Au₂₅(PhC₂S)₁₈¹² agree with the theoretical prediction. In this sense, the HOMO-LUMO gap energy as determined by measuring the absorbance edge in the near-infrared region is independent of the solvent and, therefore, this behavior parallels that observed by electrochemical means. On the other hand, important changes were observed for Au₂₅(PhC₂S)₁₈ upon oxidation either electrochemically¹² or in air⁴⁴ that agree with the core as the origin of the optical signals.

Conclusions

We demonstrated that two nearly monodisperse fractions of Au₂₅(SC₆)₁₈ and Au₁₄₄(SC₆)₅₉ nanoclusters can be prepared by maintaining the temperature of synthesis constant at 4 °C and controlling the stirring speed during the reduction process. The cluster's size and monodispersity of these fractions were determined by TEM and electrochemical means, proving that these methods and in particular electrochemistry are powerful tools to assay these nanoclusters properties.

Cyclic voltammetry, microelectrode voltammetry, and electrochemical impedance spectroscopy of the isolated two first oxidation processes of Au₂₅(SC₆)₁₈ nanoclusters allowed us to determine the electron transfer rate constants and the diffusion coefficients of the monoanionic and neutral Au₂₅(SC₆)₁₈ species.

Finally, the study of the effects of solvent in a wide range of relative permittivities showed that the model of Girault et al.¹⁶ that takes into account that the metallic core protected by an organic monolayer is also affected by the solvent nature is appropriate to describe this phenomenon. However, in cases where the relative permittivities of the solvent and the monolayer are similar, the ion penetration is facilitated¹⁸ and the charging energy values differ from the value predicted by the model. The solvent effects can be observed in the charging energy but do not influence the HOMO-LUMO gap energy as determined through the electrochemical as well as the optical measurements.

Acknowledgment. We thank the Ministerio de Educación y Ciencia (MEC) (Project CTQ2007-62723/BQU) Junta de Andalucía and University of Córdoba for financial support of this work. D.G.-R. acknowledges the MEC for a fellowship of the FPI program.

References and Notes

(1) Murray, R. W. *Chem. Rev.* **2008**, *108*, 2688.

- (2) Antonello, S.; Holm, A. H.; Instuli, E.; Maran, F. *J. Am. Chem. Soc.* **2007**, *129*, 9836.
- (3) Jimenez, V. L.; Georganopoulos, D. G.; White, R. J.; Harper, A. S.; Mills, A. J.; Lee, D. I.; Murray, R. W. *Langmuir* **2004**, *20*, 6864.
- (4) Garcia-Morales, V.; Mafe, S. *J. Phys. Chem. C* **2007**, *111*, 7242.
- (5) Quinn, B. M.; Liljeroth, P.; Ruiz, V.; Laaksonen, T.; Kontturi, K. *J. Am. Chem. Soc.* **2003**, *125*, 6644.
- (6) Miles, D. T.; Leopold, M. C.; Hicks, J. F.; Murray, R. W. *J. Electroanal. Chem.* **2003**, *554*, 87.
- (7) Toikkanen, O.; Ruiz, V.; Ronholm, G.; Kalkkinen, N.; Liljeroth, P.; Quinn, B. M. *J. Am. Chem. Soc.* **2008**, *130*, 11049.
- (8) Donkers, R. L.; Lee, D.; Murray, R. W. *Langmuir* **2004**, *20*, 1945.
- (9) Heaven, M. W.; Dass, A.; White, P. S.; Holt, K. M.; Murray, R. W. *J. Am. Chem. Soc.* **2008**, *130*, 3754.
- (10) Hakkinen, H.; Walter, M.; Gronbeck, H. *J. Phys. Chem. B* **2006**, *110*, 9927.
- (11) Whetten, R. L.; Price, R. C. *Science* **2007**, *318*, 407.
- (12) Lee, D.; Donkers, R. L.; Wang, G. L.; Harper, A. S.; Murray, R. W. *J. Am. Chem. Soc.* **2004**, *126*, 6193.
- (13) Guo, R.; Georganopoulos, D.; Feldberg, S. W.; Donkers, R.; Murray, R. W. *Anal. Chem.* **2005**, *77*, 2662.
- (14) Guo, R.; Murray, R. W. *J. Am. Chem. Soc.* **2005**, *127*, 12140.
- (15) Holm, A. H.; Ceccato, M.; Donkers, R. L.; Fabris, L.; Pace, G.; Maran, F. *Langmuir* **2006**, *22*, 10584.
- (16) Su, B.; Zhang, M. Q.; Shao, Y. H.; Girault, H. H. *J. Phys. Chem. B* **2006**, *110*, 21460.
- (17) Su, B.; Girault, H. H. *J. Phys. Chem. B* **2005**, *109*, 23925.
- (18) Laaksonen, T.; Pelliniemi, O.; Quinn, B. M. *J. Am. Chem. Soc.* **2006**, *128*, 14341.
- (19) Brust, M.; Walker, M.; Bethell, D.; Schiffrin, D. J.; Whyman, R. *J. Chem. Soc., Chem. Commun.* **1994**, 801.
- (20) Brauer, G. *Handbook of Preparative Inorganic Chemistry*; Academic Press: New York, 1965.
- (21) Nicholson, R. S. *Anal. Chem.* **1965**, *37*, 1351.
- (22) Miles, D. T.; Murray, R. W. *Anal. Chem.* **2003**, *75*, 1251.
- (23) Hicks, J. F.; Miles, D. T.; Murray, R. W. *J. Am. Chem. Soc.* **2002**, *124*, 13322.
- (24) Kim, J.; Lema, K.; Ukaigwe, M.; Lee, D. *Langmuir* **2007**, *23*, 7853.
- (25) Donkers, R. L.; Lee, D.; Murray, R. W. *Langmuir* **2008**, *24*, 5976.
- (26) Shibu, E. S.; Muhammed, M. A. H.; Tsukuda, T.; Pradeep, T. *J. Phys. Chem. C* **2008**, *112*, 12168.
- (27) Zhu, M.; Aikens, C. M.; Hollander, F. J.; Schatz, G. C.; Jin, R. *J. Am. Chem. Soc.* **2008**, *130*, 5883.
- (28) Chaki, N. K.; Negishi, Y.; Tsunoyama, H.; Shichibu, Y.; Tsukuda, T. *J. Am. Chem. Soc.* **2008**, *130*, 8608.
- (29) Negishi, Y.; Chaki, N. K.; Shichibu, Y.; Whetten, R. L.; Tsukuda, T. *J. Am. Chem. Soc.* **2007**, *129*, 11322.
- (30) Tracy, J. B.; Kalyuzhny, G.; Crowe, M. C.; Balasubramanian, R.; Choi, J. P.; Murray, R. W. *J. Am. Chem. Soc.* **2007**, *129*, 6706.
- (31) Zhu, M.; Lanni, E.; Garg, N.; Bier, M. E.; Jin, R. *J. Am. Chem. Soc.* **2008**, *130*, 1138.
- (32) Shichibu, Y.; Negishi, Y.; Tsukuda, T.; Teranishi, T. *J. Am. Chem. Soc.* **2005**, *127*, 13464.
- (33) Shichibu, Y.; Negishi, Y.; Tsunoyama, H.; Kanehara, M.; Teranishi, T.; Tsukuda, T. *Small* **2007**, *3*, 835.
- (34) Georganopoulos, D. G.; Mirkin, M. V.; Murray, R. W. *Nano Lett.* **2004**, *4*, 1763.
- (35) Peterson, R. R.; Cliffel, D. E. *Langmuir* **2006**, *22*, 10307.
- (36) Templeton, A. C.; Wuelfing, M. P.; Murray, R. W. *Acc. Chem. Res.* **2000**, *33*, 27.
- (37) Pietron, J. J.; Hicks, J. F.; Murray, R. W. *J. Am. Chem. Soc.* **1999**, *121*, 5565.
- (38) Quinn, B. M.; Liljeroth, P.; Kontturi, K. *J. Am. Chem. Soc.* **2002**, *124*, 12915.
- (39) Parker, J. F.; Choi, J.-P.; Wang, W.; Murray, R. W. *J. Phys. Chem. C* **2008**, *112*, 13976.
- (40) Lide, D. R. *CRC Handbook of Chemistry and Physics*, 86th ed.; CRC Press: Boca Raton, FL, 2005.
- (41) Brandrup, J.; Immergut, E. H.; Grulke, E. A. *Polymer Handbook*, 4th ed.; Wiley: New York, 1999.
- (42) Huang, S. H.; Minami, K.; Sakaue, H.; Shingubara, S.; Takahagi, T. *J. Appl. Phys.* **2002**, *92*, 7486.
- (43) Pei, L. H.; Mori, K.; Adachi, M. *Colloids Surf., A* **2006**, *281*, 44.
- (44) Zhu, M. Z.; Eckenhoff, W. T.; Pintauer, T.; Jin, R. C. *J. Phys. Chem. C* **2008**, *112*, 14221.
- (45) Aikens, C. M. *J. Phys. Chem. C* **2008**, *112*, 19797.

JP901118T